Tight Coupling of Astrocyte pH Dynamics to Epileptiform Activity Revealed by Genetically-Encoded pH Sensors

Joseph V. Raimondo[1, 2, 3], Hayley Tomes[2], Agnese Irkle[1], Louise Kay[1], Lauriston Kellaway[2], Henry Markram[4], Robert P. Millar[3,5], Colin J. Akerman[1]

[1]Department of Pharmacology, University of Oxford, Oxford, United Kingdom
[2]Division of Physiology, Department of Human Biology, Faculty of Health Sciences, University of Cape Town, Cape Town, South Africa
[3]UCT/MRC Receptor Biology Unit, Department of Integrative Biomedical Sciences and Institute of Infectious Disease and Molecular Medicine, Faculty of Health Sciences, University of Cape Town, Cape Town, South Africa
[4]Brain Mind Institute, École Polytechnique Fédérale de Lausanne, Lausanne, Switzerland
[5]Centre for Neuroendocrinology and Mammal Research Institute, University of Pretoria, Pretoria, South Africa

Correspondence:
Colin J. Akerman, PhD
Department of Pharmacology
Oxford University
Oxford, Mansfield Road, OX1 3QT
email: colin.akerman@pharm.ox.ac.uk

Running Title
Rapid astrocyte pH dynamics coupled to epileptiform activity

Keywords
Intracellular pH, astrocytes, epileptiform activity, seizures

Acknowledgements
This work was supported by a grant from the Medical Research Council (G0601503), the Oxford Stem Cell Institute and the Blue Brain Project. The research leading to these results has received funding from the European Research Council under the European Community's Seventh Framework Programme (FP7/2007-2013), ERC grant agreement number 243273 and 617670. In addition, this work was supported by equipment from the École Polytechnique Fédérale de Lausanne, Switzerland. J.V.R was supported by a Rhodes Scholarship, a NRF Innovation Postdoctoral Fellowship, a UCT URC Postdoctoral Fellowship and a Royal Society Newton Advanced Fellowship.

Significance Statement

Dynamic changes in intracellular ion concentrations are central to the initiation and progression of epileptic seizures. However, it is not known how changes in intracellular H+ concentration (i.e. pH) differ between different cell types during seizures. Using recently developed pH-sensitive proteins, we demonstrate that astrocytes undergo rapid alkalinization during periods of seizure-like activity, which is in stark contrast to the acidification that occurs in neighboring neurons. Rapid astrocytic pH changes are highly temporally correlated with seizure activity, are mediated by an electrogenic Na+/HCO3- cotransporter, and are more tightly coupled to network activity than are neuronal pH changes. As pH has profound effects on signaling in the nervous system, this work has implications for our understanding of seizure dynamics.

Abstract

Astrocytes can both sense and shape the evolution of neuronal network activity and are known to possess unique ion regulatory mechanisms. Here we explore the relationship between astrocytic intracellular pH dynamics and the synchronous network activity that occurs during seizure-like activity. By combining confocal and two-photon imaging of genetically-encoded pH reporters with simultaneous electrophysiological recordings, we perform pH measurements in defined cell populations and relate these to ongoing network activity. This approach reveals marked differences in the intracellular pH dynamics between hippocampal astrocytes and neighboring pyramidal neurons in rodent in vitro models of epilepsy. With three different genetically-encoded pH reporters,

astrocytes are observed to alkalinize during epileptiform activity, whilst neurons are observed to acidify. In addition to the direction of pH change, the kinetics of epileptiform-associated intracellular pH transients are found to differ between the two cell types, with astrocytes displaying significantly more rapid changes in pH. The astrocytic alkalinization is shown to be highly correlated with astrocytic membrane potential changes during seizure-like events and mediated by an electrogenic Na^+/HCO_3^- cotransporter. Finally, comparisons across different cell-pair combinations reveal that astrocytic pH dynamics are more closely related to network activity than are neuronal pH dynamics. This work demonstrates that astrocytes exhibit distinct pH dynamics during periods of epileptiform activity, which has relevance to multiple processes including neurometabolic coupling and the control of network excitability.

Introduction

Astrocytes are deeply interwoven into the fabric of neuronal circuits, where they play active roles in modulating the function and computation of networks (Araque et al., 1999). One of the primary mechanisms that astrocytes contribute to is ion homeostasis, which is essential for chemical and electrical signaling in the brain (Walz, 2000). In addition, astrocytes are known to continually regulate the delivery of energy substrates to neurons (Bittner et al., 2011; Choi et al., 2012; Pellerin and Magistretti, 1994). These processes become particularly important during periods of intense neural activity, such as occur in epileptic seizures. Seizure activity represents a significant challenge to ion homeostasis and can result in pronounced changes in intracellular and extracellular ion concentrations, which are also associated with an increase in the tissue's metabolic demands (Dreier and Heinemann, 1991; Howarth et al., 2012; Raimondo et al., 2015). The central involvement of astrocytes in these processes is highlighted by evidence that altered potassium handling by astrocytes can be pro-epileptic (Bedner et al., 2015; Hinterkeuser et al., 2000; Wallraff et al., 2006) and that calcium elevations in astrocytes sustain seizure-like activity (Gomez-Gonzalo et al. 2010).

Changes in pH, the negative logarithm of H^+ ion concentration, have also been associated with seizure activity. Neurons for instance, have been shown to experience intracellular acidification (Raimondo et al., 2012; Xiong et al., 2000), which is likely to feedback into ongoing seizure activity because neuronal excitability, synaptic transmission and the availability of energy substrates are all known to exhibit pH

104 sensitivity (Erecińska et al., 1995; Taira et al., 1993; Traynelis and Cull-Candy, 1990).
105 Meanwhile, although astrocytic pH dynamics during seizure activity have received less
106 attention, it is well established that pH regulation mechanisms differ in glial cells. In
107 response to sustained membrane depolarization for example, astrocytes exhibit
108 intracellular alkalinization as opposed to acidification (Ahmed and Connor, 1980;
109 Boyarsky et al., 1988a; Chesler and Kraig, 1989; Deitmer and Szatkowski, 1990). This
110 is consistent with evidence that astrocytes exhibit distinct pH regulatory mechanisms
111 compared to neurons, including electrogenic transport mechanisms that provide a direct
112 link between membrane depolarization and bicarbonate/proton fluxes, particularly via
113 the action of the electrogenic sodium-bicarbonate cotransporter NBCe1 (Bevensee,
114 1997; Boyarsky et al., 1993; Brookes and Turner, 1994; Pappas and Ransom, 1994;
115 Ruminot et al., 2011a; Theparambil et al., 2014).
116
117 A prediction therefore is that astrocytes experience alkaline shifts during epileptiform
118 activity and that the kinetics of the pH dynamics in astrocytes may be different to those
119 in neurons. Previous work has used ion-sensitive electrodes and dyes to monitor pH
120 dynamics in astrocytes (Chesler and Kraig, 1989; Theparambil et al., 2014). The recent
121 development of genetically-encoded reporters now provides a series of different pH-
122 sensitive proteins that can be delivered to cell types within intact brain preparations.
123 These tools make it possible to monitor pH in distinct cell types, either by using
124 molecular, morphological and/or functional features to classify individual cells at the
125 time of recording (Benediktsson et al., 2005; Bizzarri et al., 2009). In this study we
126 combine genetically-encoded pH reporters with simultaneous whole-cell patch clamp

recordings to observe cell-type specific pH responses during seizure-like events (SLEs) in vitro. By measuring pH dynamics in astrocytes across different models of epilepsy, we demonstrate that astrocytes exhibit pronounced intracellular alkaline pH shifts during epileptiform activity. Furthermore, we show that the kinetics of the pH dynamics differ significantly across cell types and that astrocytic pH changes are actually more tightly coupled to the network activity than are the pH changes in neurons.

136 *Materials and methods*
137

138 Slice preparation and DNA transfection

139 Rat organotypic hippocampal slice cultures were prepared using a method similar to
140 that described by Stoppini and colleagues (Stoppini et al., 1991). Briefly, 7 day old male
141 Wistar rats were killed in accordance with the UK Animals Scientific Procedures Act
142 1986. The brains were extracted and placed in cold (4 °C) Geys Balanced Salt Solution
143 (GBSS), supplemented with D-glucose (34.7 mM). All reagents were purchased from
144 Sigma-Aldrich, unless stated otherwise. The hemispheres were separated and
145 individual hippocampi were removed and immediately sectioned into 350 µm thick slices
146 on a McIlwain tissue chopper. Slices were rinsed in cold dissection medium, placed
147 onto Millicell-CM membranes and maintained in culture medium containing 25 % EBSS,
148 50 % MEM, 25 % heat-inactivated horse serum, glucose, and B27 (Invitrogen). Slices
149 were incubated at 36 °C in a 5 % CO_2 humidified incubator before transfection. Neurons
150 were biolistically transfected after 4-7 days in vitro using a Helios Gene Gun (120 psi;
151 Bio-Rad). The target DNA was either E^2GFP as part of pcDNA3-ClopHensor
152 (generously provided by Daniele Arosio, University of Trento; Addgene plasmid #25938)
153 or ClopHensorN (Raimondo et al., 2013; Addgene plasmid #50758), deGFP4 in
154 pEGFP-N1 (generously provided by Jim Remington, University of Oregon), or Cl-sensor
155 in pEGFP-C1 (generously provided by Piotr Bregestovski, INMED, Marseille). 50 µg of
156 target DNA was precipitated onto 25 mg of 1.6 µm diameter gold microcarriers and
157 bullets generated in accordance with the manufacturer's instructions (Bio-Rad). This
158 resulted in sparse transfection rates (typically less than 10 cells per slice) and

recordings were performed 2-7 days post-transfection. At the time of recording therefore, transfected cells were comparable to postnatal day 13-21.

Electrophysiological recordings and activity-dependent manipulations

Organotypic hippocampal slices were transferred to a recording chamber and continuously superfused with 95% O_2/ 5% CO_2 oxygenated ACSF, warmed to 32-35 °C. The composition of the 'standard' ACSF was (in mM): NaCl (120), KCl (3), $MgCl_2$ (2), $CaCl_2$ (2), NaH_2PO_4 (1.2), $NaHCO_3$ (23), D-Glucose (11). The pH was adjusted to be between 7.35 and 7.40 using NaOH. Seizure like events (SLEs) occurred following the exchange of normal ACSF to nominally Mg^{2+}-free ACSF (Anderson et al., 1986) (Mg^{2+} omitted from standard ACSF) or nominally Cl^--free ACSF (Yamamoto and Kawai, 1967) (NaCl, $MgCl_2$ and $CaCl_2$ of standard ACSF replaced with 120 mM sodium D-gluconate, 1 mM $MgSO_4$ and 3 mM calcium D-gluconate, respectively). In some experiments, HCO_3^- was removed from the Cl^--free ACSF by substituting $NaHCO_3$ with an equimolar concentration of HEPES, and oxygenating with 100% O_2. As it is difficult to completely remove HCO_3^-, due to the fact that CO_2 is continuously generated and rapidly converted to HCO_3^- by carbonic anhydrases, we refer to this as a low HCO_3^- ACSF. Brain slices were maintained in the relevant SLE-inducing ACSF (i.e. 0 Mg^{2+} or 0 Cl^-) before pH imaging began. Patch pipettes of 3-5 MΩ tip resistance were pulled from filamental borosilicate glass capillaries (1.2 mm outer diameter, 0.69 mm inner diameter; Harvard Apparatus Ltd), using a horizontal puller (Sutter P-97 or P-1000). For whole-cell recordings, pipettes were filled with an internal solution containing (in mM): K-gluconate

(126), Na_2ATP (4), NaGTP (0.3), Na_2-phosphocreatine (10), KCl (4), and HEPES (10). The osmolarity of internal solutions was adjusted to 290 mOsM and the pH was adjusted to 7.38 with KOH. Pyramidal neurons or astrocytes within the CA1 and CA3 regions were visualized under 40x or 60x water-immersion objectives (Leica or Olympus) and targeted for recording. Patch-clamp recordings were made using Axopatch 1D, Axopatch 200B or Axoclamp 2B amplifiers (Axon Instruments). Data was acquired with WinWCP Strathclyde Whole Cell Analysis software (V.3.9.7; University of Strathclyde) or PulseQ running on IGOR (Funetics), before being exported to the MATLAB environment (MathWorks) for further analysis using customized scripts.

Imaging and calibrating intracellular pH measurements

Concurrent with electrophysiological recordings, the intracellular pH of a transfected CA1/CA3 pyramidal neuron and/or astrocyte was measured using the following imaging techniques. For E^2GFP-expressing cells, imaging was performed using an upright Leica SP2 AOBS laser scanning confocal microscope equipped with a 40x water immersion objective (NA 0.8). Sequential excitation of E^2GFP at 458 nm and 488 nm was achieved with a multi-line argon laser. Emitted fluorescence was detected between 500 nm and 550 nm using a single photomultiplier tube (PMT) at a constant voltage. To compensate for fluctuations in laser intensity, a custom built laser power sensor (sample rate 10 kHz) was used to record laser power output during imaging (Arosio et al., 2010; Zucker and Price, 2001) and the resulting data was used to correct fluorescence ratios offline. For deGFP4 and Cl-sensor-expressing neurons, imaging was performed using

an Olympus FV300 confocal microscope (Olympus, Japan), custom-converted for two-photon imaging and equipped with a MaiTai-HP Ti:sapphire femtosecond pulsed laser (Newport Spectra-Physics, USA). Images were acquired on a PC using Fluoview software (version 5.0, Olympus, Japan). The two-photon system was mounted on an Olympus BX51 upright microscope equipped with a 40x water immersion objective (NA 0.80). Fluorescence was detected using two externally mounted PMTs (R3896, Hamamatsu, Japan). An excitation wavelength of 810 nm or 850 nm was used for deGFP4 or Cl-sensor, respectively. Emitted fluorescence from deGFP4 was separated using a dichroic mirror at 495 nm and filtered for detection by the two PMTs at 450-490 nm and 500-550 nm. Emitted fluorescence from Cl-sensor was separated using a dichroic mirror at 510 nm before being filtered for detection at 460-500 nm and 520-550 nm. Images were exported to the MATLAB environment where background was subtracted and fluorescence measurements were made from regions of interest selected over the soma of individual cells. Excitation or emission fluorescence ratios (R_{pH}) were converted to pH according to calibration curves collected for each construct.

For the calibration, intracellular pH was controlled by equilibrating extra- and intracellular ion concentrations using the K^+/H^+ exchanger nigericin (10μM) and the Cl^-/OH^- exchanger tributyltinchloride in a high K^+ ACSF containing (in mM) potassium D-gluconate (123), HEPES (23), D-glucose (11), NaH_2PO_4 (1.2), MgSO4 (2) and calcium D-gluconate (2) (Boyarsky et al., 1988a). pH was adjusted with small aliquots of NaOH and, to avoid CO_2 dependent pH buffering, ACSF was bubbled with 100 % O_2. For each

indicator, either an excitation (E^2GFP) or emission (deGFP4, Cl-sensor) fluorescence ratio (R) was measured at different intracellular pHs:

$$R = {}^{S_N}/_{S_D}$$

Where S_N and S_D were the numerator and denominator of the calculated fluorescence ratio, respectively. The formation of a 1:1 analyte-sensor complex results in an equilibrium described by the Grynkiewicz equation (Arosio et al., 2010; Grynkiewicz et al., 1985), which can be written as follows:

$$pH_i = pK_a + \log\left(\frac{R - R_A}{R_B - R}\right) + \log\left(\frac{S_{D,A}}{S_{D,B}}\right)$$

R_A and R_B are the values of R for the ratiometric indicator in its most acidic and basic forms, respectively. Likewise, $S_{D,A}$ and $S_{D,B}$ reflect S_D in its acidic and basic form. pK_a is the acid dissociation constant of the indicator. Calibration data was fitted using the following rearranged version of the above equation:

$$R = \frac{R_B 10^{pH - pK_A - \log(\frac{S_{D,A}}{S_{D,B}})} + R_A}{1 + 10^{pH - pK_A - \log(\frac{S_{D,A}}{S_{D,B}})}}$$

This allowed the pKa of each construct to be determined and intracellular pH to be calculated from measured fluorescence ratios (R) during subsequent experiments. Calibration curves were constructed from fluorescence measurements that were averaged over a population of 'pH-clamped' cells. As with other ratiometric reporters, this means that there is an inherent variance when pH values are assigned to individual cells, but that relative changes in pH (i.e. within-cell changes) are not affected by this

source of variance. Some of the data generated for the calibration of the genetic reporters was used in a previous study (Raimondo et al. 2012).

For pH imaging, astrocytes were identified by their morphology and location (within stratum radiatum). Two broad morphological groups were observed, the first included cells with small somata and multiple fine processes (protoplasmic astrocytes). The second group included multipolar cells with irregularly shaped, elongated somata, with more than two large processes emanating in different directions (fibrous astrocytes). These two groups are consistent with a detailed description of the morphologies observed for GFAP-positive astrocytes in the hippocampus (Benediktsson et al., 2005). To further confirm the accuracy of the identification of astrocytes using morphological criteria, a subset of our cells were targeted for whole cell patch recording. In all cases (n = 9 out of 9 cells), a low resting membrane potential (-75 ± 8.6 mV), low membrane resistance (32.5 ± 1.9 MΩ) and the inability to fire action potentials was confirmed, consistent with previous data (McKhann et al., 1997; O'Connor et al., 1994). These electrophysiological properties were consistent with our morphological classification of the cells as astrocytes.

Data analysis and statistics

All data are presented as means ± SEM. Statistical tests were either performed using the Statistics toolbox in MATLAB or GraphPad Prism version 5.0 (GraphPad Software) (* $p<0.05$, ** $p<0.01$, *** $p<0.0001$). Data were tested for normality using a Kolmogorov–

Smirnov test and the appropriate statistical tests were applied. To assess the degree of correlation between current clamp recordings and pH imaging traces, the membrane potential recordings were resampled to match the sampling rate of the pH imaging.

Results

Astrocytes experience rapid intracellular alkalinization during SLEs

In order to compare pH dynamics in astrocytes and neurons during epileptiform network activity we delivered the genetically-encoded pH sensor, E^2GFP, to the different cell types within the same hippocampal slice (**Fig. 1a, b**). Using biolistic transfection methods we were able to sparsely transfect cells within organotypic hippocampal slice cultures. This meant that E^2GFP-exressing CA1/CA3 pyramidal neurons and astrocytes could be easily distinguished by their distinctive morphology and location (Benediktsson et al., 2005; see *Materials and methods*). In order to confirm the accuracy of the identification of astrocytes from morphological criteria, a subset of cells were also targeted for whole-cell patch clamp recordings and characterized electrophysiologically. In all cases (n = 9 out of 9 cells), a low resting membrane potential (-75 ± 8.6 mV), low membrane resistance (32.5 ± 1.9 MΩ) and inability to fire action potentials was confirmed (**Fig. 1c**). Concurrent with pH imaging, SLEs elicited by Mg^{2+} free ACSF were monitored via whole-cell patch clamp recordings from CA1/CA3 pyramidal neurons. These electrophysiological measurements were made from a nearby pyramidal neuron (somata within 200 μm) so as to avoid disrupting pH regulatory mechanisms in the imaged cell (**Fig. 1a, b**). Interestingly, the pH_i before the onset of SLEs was found to be significantly different between neurons and astrocytes. The pre-SLE pH_i in neurons was relatively more alkaline at 7.69 ± 0.30 (n = 23), whereas the pre-SLE pH_i was relatively more acidic in astrocytes at 7.28 ± 0.32 (n = 22; $P < 0.0001$, t test, **Fig. 1d**). The two cell

types also differed substantially in their pH dynamics during epileptiform activity. SLEs resulted in a highly significant intracellular acidic shift in neurons ($P < 0.0001$, *t* test, $n = 101$ events from 23 neurons, **Fig. 1a**). In stark contrast to neurons, astrocytes exhibited strong and rapid intracellular alkalinization during periods of epileptiform activity ($P < 0.0001$, *t* test, $n = 112$ events from 24 astrocytes, **Fig. 1b, c, e**). Even short synchronous network events caused detectable shifts in intracellular pH (**Fig. 1a, b, e**). For instance, events lasting 1-3 s caused a peak decrease of 0.016 ± 0.01 pH units in neurons ($P = 0.0002$, *t* test) and a peak increase of 0.047 ± 0.04 pH units in astrocytes ($P = 0.0012$, *t* test). Furthermore, the magnitude of intracellular pH changes was well correlated with the length of the recorded SLE ($r = -0.67$ for neurons and $r = 0.58$ for astrocytes, $P < 0.0001$, Pearson Correlation, **Fig. 1e**). The slope of the linear fit for peak change in intracellular pH in neurons revealed a decrease of 0.007 pH units per second of epileptiform activity. For astrocytes, the peak change in intracellular pH as a function of SLE duration was best fit by a single phase exponential with a plateau of 0.18 pH units and a time constant 14.7 s (**Fig. 1e**).

Different genetically-encoded pH sensors confirm astrocytic alkalinization during different models of epileptic seizures

In order to confirm our observation of epileptiform activity-induced alkaline transients in astrocytes, we utilized three different genetically-encoded pH-sensitive probes and two

317 separate in vitro models of epileptic seizures (**Fig. 2** and **Fig. 3**). The reporters E^2GFP,
318 deGFP4 and Cl-sensor were calibrated by systematically varying extracellular pH in the
319 presence of a proton permeable ionophore in order to achieve known intracellular pH
320 values (see *Materials and Methods*). E^2GFP was used as a ratiometric pH indicator by
321 excitation, whilst deGFP4 and Cl-sensor were used as ratiometric pH indicators by
322 emission (see *Materials and Methods*). The fluorescence ratios were shown to depend
323 on intracellular pH with a pKa of 7.6 for E^2GFP, 7.4 for deGFP4 and 7.7 for Cl-sensor
324 (**Fig. 2a, b, c**). Both E^2GFP and deGFP4 demonstrated reliable astrocytic alkaline
325 transients in response to 0 Mg^{2+} induced SLEs (**Fig. 1b** and **Fig. 2d**). In addition,
326 epileptiform activity could also be elicited by removing Cl^- from the ACSF, which has
327 been established as a model of epileptic seizures (Yamamoto, 1972). Removal of Cl^-
328 from the ACSF has the added advantage of preventing potential Cl^- fluxes that would
329 complicate pH measurements from the pH and Cl^- sensitive genetic reporter Cl-sensor
330 (Markova et al., 2008; Raimondo et al., 2012). Intracellular pH measurements made
331 using both E^2GFP and Cl-sensor in nominally Cl^- free ACSF also revealed alkalinization
332 in response to SLEs (**Fig. 2e, f**).
333
334 At a population level, when we compared peak changes in intracellular pH during SLEs
335 (20-40 s in duration), we observed a highly significant difference between neurons and
336 astrocytes for each pH reporter or seizure model (E^2GFP 0 Mg^{2+}: -0.24 ± 0.03 pH unit
337 shift in neurons vs. 0.15 ± 0.01 pH unit shift in astrocytes, $P < 0.0001$, E^2GFP 0 Cl^-: -
338 0.33 ± 0.02 vs. 0.27 ± 0.01 pH units, $P < 0.0001$, DeGFP4 0 Mg^{2+}: -0.23 ± 0.03 vs. 0.20
339 ± 0.04 pH units, $P < 0.0001$, Cl-sensor 0 Cl^-: -0.19 ± 0.01 vs. 0.13 ± 0.01 pH units, $P <$

0.0001, *t* test, **Fig. 3a, b, c, d**). These experiments confirm that genetically-encoded pH reporters are able to detect robust intracellular acidification of hippocampal neurons and intracellular alkalinization of hippocampal astrocytes during epileptiform activity.

Epileptiform activity-induced alkaline transients in astrocytes are mediated by depolarization and the sodium-bicarbonate co-transporter NBCe1.

Given the presence of markedly different activity-dependent pH dynamics in astrocytes compared to neurons, we sought to explore in further detail how SLEs relate to the observed pH transients in astrocytes. First, we performed dual whole-cell current clamp recordings to confirm that 0 Mg^{2+} ACSF elicits SLEs that constitute synchronous, highly-correlated periods of activity between principal hippocampal neurons. Consistent with previous findings (Ellender et al., 2014), we observed a high mean linear correlation in the membrane potential of pairs of pyramidal neurons during SLEs (r = 0.91 ± 0.01, n = 20 SLEs from 7 pairs of neurons, Pearson Correlation; **Fig. 4a, c**). Next, we examined how the membrane potential of astrocytes relates to the epileptiform network activity. To do this we performed simultaneous current clamp recordings from a pyramidal neuron and a nearby astrocyte (somata within 200 µm). The identity of the astrocyte was again confirmed by their hyperpolarized resting membrane potential (-77.4 ± 1.5 mV), low input resistance (80.9 ± 42.7 MΩ) and lack of voltage-gated conductances, consistent with previous reports (McKhann et al., 1997; O'Connor et al., 1994). In comparison,

363 recorded neurons were able to generate action potentials and had a resting membrane
364 potential of -60.3 ± 2.1 mV and an input resistance of 201.7 ± 39.8 MΩ. During
365 epileptiform activity we observed that although the range of membrane potential values
366 was narrower for the astrocyte, the seizure-associated membrane depolarizations
367 occurred synchronously in astrocytes and pyramidal neurons (**Fig. 4b**). As a result, the
368 astrocytic membrane potential was also observed to be highly correlated with the
369 pyramidal neuron membrane potential during SLEs (r = 0.80 ± 0.02, n = 14 SLEs from 9
370 pairs of cells, Pearson Correlation, **Fig. 4c**).
371
372 These epileptiform-induced depolarizations of the astrocyte membrane potential would
373 be predicted to generate alkalinization via the electrogenic sodium-bicarbonate
374 cotransporter NBCe1, and could therefore account for the alkaline shifts observed with
375 our pH reporters (Bevensee, 1997; Majumdar and Bevensee, 2010). To test this, we
376 examined whether astrocytic alkalinization during SLEs was sensitive to S0859, an N-
377 cyanosulphonamide inhibitor of sodium-bicarbonate cotransport (Ch'en et al., 2008;
378 Ruminot et al., 2011b). Bath application of 50 µM S0859 did not affect the intracellular
379 pH of astrocytes measured before SLE onset. The pre-SLE pH was 7.29 ± 0.034 in
380 control astrocytes and the pre-SLE was 7.30 ± 0.04 in S0859-treated astrocytes (P =
381 0.79, t-test). However, S0859 markedly reduced SLE-associated alkaline transients in
382 astrocytes (**Fig. 4d, e**). In S0859-treated astrocytes, 0 Mg^{2+} induced SLEs resulted in an
383 alkaline transient of just 0.02 ± 0.01 pH units, which was significantly smaller than the
384 alkaline transient observed in control astrocytes of 0.13 ± 0.01 pH units (P < 0.0001, t-
385 test). Interestingly, S0859 was associated with a reduction in SLE duration (**Fig. 4f**), but

the effect of S0859 on astrocytic alkalinization was still evident when we accounted for SLE duration. When SLEs of matched duration were compared (i.e. SLEs of less than 35 s duration), S0859 significantly reduced astrocytic alkalinization from 0.11 ± 0.01 pH units under control conditions, to 0.02 ± 0.01 pH units in the presence of S0859 (P < 0.0001, t-test, **Fig. 4g**). Similarly, S0859 significantly reduced astrocytic alkalinization for 0 Cl^--induced SLEs from 0.13 ± 0.01 pH units under control conditions, to 0.05 ± 0.03 pH units in the presence of S0859 (P < 0.01, t-test, **Fig. 4g**). Finally, consistent with a bicarbonate-dependent process, the use of a low HCO_3^- ACSF also significantly reduced astrocytic alkalinization during SLEs from 0.13 ± 0.01 pH units in control ACSF, to 0.08 ± 0.02 pH units in reduced HCO_3^- ACSF (P < 0.05, t-test, **Fig. 4g**). Taken together, these data support the conclusion that sodium-bicarbonate cotransporter play a central role in the generation of epileptiform activity-induced alkalinization in hippocampal astrocytes.

<u>The kinetics of pH transients in astrocytes and neurons differ during epileptiform activity</u>

Having established that astrocytes and neurons exhibit opposing pH changes during epileptiform activity, we were keen to examine whether the dynamics of these pH changes were comparable between the two cells types. To do this we performed simultaneous or sequential pH-imaging from neurons and astrocytes within the same hippocampal brain slice. In addition, we analyzed individually recorded intracellular pH

dynamics from both cell types at a population level (**Fig. 5**). Simultaneous pH readout from these two cell types during the same SLEs was attained by rapid imaging of an astrocyte and the apical dendrite of a nearby pyramidal neuron (**Fig. 5a, b**). The examples in **Fig. 5c** and **Fig. 5d** depict sequential imaging of intracellular pH dynamics in both cell types in response to similar SLEs within the same hippocampal slice preparation. During epileptiform activity astrocytes were observed to alkalinize, whilst the neurons acidified (**Fig. 5b, c, d**). This was true for SLEs generated in 0 Mg^{2+} (**Fig. 5c**) or 0 Cl^- (**Fig. 5d**). Importantly, these recordings allowed us to observe differences in the intracellular pH kinetics between the two cell types. Astrocytes were observed to reach their peak pH change significantly more quickly than neurons (**Fig. 5b, c, d**). During 0 Mg^{2+} SLEs, the peak pH shifts in astrocytes occurred at 71.3 ± 5.2% of SLE duration (n = 25), as compared to 134.5 ± 7.7% of SLE duration in neurons (n = 30; **Fig. 5e**, $P < 0.0001$, t test). This difference was similar in 0 Cl^- events where astrocytic pH had shifted maximally by 62.4 ± 2.7% (n = 63) of SLE duration, compared to 111.4 ± 3.2% of SLE duration (n = 85) in neurons (**Fig. 5e**, $P< 0.0001$, t test). In summary, whilst astrocytes reach maximal alkalinity approximately halfway during activity SLE, neurons continue to experience increases in pH and reach their most acidic values at, or shortly after, the cessation of the SLE.

The kinetics of pH recovery following SLEs was also found to be more rapid in astrocytes (**Fig. 5b, c, d**). Astrocytes returned to baseline shortly after the end of a SLE (138.8 ± 7.5% of SLE duration in 0 Mg^{2+}, n = 25; and 136.1 ± 4.0% of SLE duration in 0 Cl^-, n = 62). In contrast, the intracellular pH of neurons took markedly longer to recover

(369.0 ± 23.0% of SLE duration in 0 Mg^{2+}, n = 21; and 311.5 ± 14.1% of SLE duration in 0 Cl^-, n = 39). This difference was highly statistically significant for both of the seizure models ($P < 0.0001$, *t* test, **Fig. 5e**). Together, these data demonstrate that the kinetics of SLE-associated intracellular pH transients are very different between astrocytes and pyramidal neurons: epileptiform pH kinetics are faster in astrocytes and slower in neurons.

Activity-dependent astrocytic pH dynamics are most tightly coupled to epileptiform activity

These data suggest that pH dynamics in astrocytes are more closely aligned with epileptiform network activity than are pH dynamics in neurons. To address this directly we performed simultaneous electrophysiological recordings and intracellular pH measurements from different combinations of cell types (**Fig. 6**). This enabled us to quantify the correlation between the pH and the membrane potential of different cell types during epileptiform activity (**Fig. 7a**). Consistent with our observation that astrocytic alkalinization is mediated by the electrogenic cotransporter NBCe1 (**Fig. 4**), we observed a very high correlation between astrocytic pH and astrocytic membrane potential (r = 0.71 ± 0.02, n = 28; **Fig. 6a** and **Fig. 7a**). In fact, we observed that the correlation between astrocytic pH and neuronal membrane potential (r = 0.43 ± 0.04, n

454 = 40) was significantly greater than the correlation between neuronal -pH and neuronal
455 membrane potential (r = 0.15 ± 0.05, n = 44; P < 0.0001, *t* test; **Fig. 6b, c** and **Fig. 7a**).
456
457 This indicates that astrocytic pH is more tightly coupled to epileptiform activity, although
458 it remained a possibility that neuronal -pH was actually more highly correlated, but was
459 offset in time with respect to network activity. To test this, we calculated the cross
460 correlation between the different signals by shifting the pH recording in time, relative to
461 the membrane potential recording (**Fig. 7b**). Consistent with the pH changes occurring
462 in response to network activity, the maximum cross correlations were observed when
463 pH measurements were shifted with a negative lag. Again, we found that the maximum
464 cross correlation coefficient was the highest between astrocytic pH and astrocytic
465 membrane potential (r = 0.77 ± 0.02, n = 28; **Fig. 7c**). Furthermore, the maximum cross
466 correlation between astrocyte pH and neuronal membrane potential (*r* = 0.68 ± 0.02, n =
467 40; **Fig. 7c**) was significantly greater than the maximum cross correlation between
468 neuronal -pH and neuronal membrane potential (r = 0.45 ± 0.04, n = 44; P < 0.0001, *t*
469 test; **Fig. 7c**). Taken together, these data show that the pH changes in astrocytes are
470 more tightly coupled to the epileptiform network dynamics, than are pH changes in
471 neurons.
472
473

Discussion

Here we have used genetically-encoded pH indicators in conjunction with confocal and two-photon microscopy in order to measure intracellular pH dynamics during epileptiform activity in rat organotypic hippocampal slice cultures. This approach has enabled us to confirm that cell-specific differences in pH regulatory mechanisms result in marked differences in intracellular pH dynamics between hippocampal astrocytes and hippocampal pyramidal neurons. In two in vitro models of seizure activity, and with three different genetically-encoded pH reporters, astrocytes were observed to alkalinize during SLEs, whilst neurons were observed to acidify. In addition to the direction of pH change, the kinetics of epileptiform-associated intracellular pH transients were found to differ between the two cell types, with astrocytes displaying significantly more rapid changes in pH. The astrocytic alkalinization during epileptiform activity was shown to be mediated by an electrogenic Na^+/HCO_3^- cotransporter and the kinetics of intracellular pH changes meant that the astrocytic pH tracked ongoing network activity more closely than the neuronal pH.

Our use of genetic reporters to measure intracellular pH compliments earlier studies using ion-sensitive pH electrodes and pH-sensitive dyes, which have provided important information regarding pH regulation in the nervous system (Ahmed and Connor, 1980; Boyarsky et al., 1988b, 1993; Chesler and Kraig, 1989; Deitmer and Szatkowski, 1990; Pappas and Ransom, 1994; Rose and Deitmer, 1995). Genetic reporters of pH offer potential advantages including the opportunity to be targeted to specific cell populations,

497 sparse labelling that can facilitate the visualization of cell morphologies and stable
498 imaging over extended time periods. Our quantification of cell-specific differences in the
499 direction and kinetics of activity-associated pH dynamics were strengthened by the fact
500 that we observed comparable results with three different genetically-encoded pH
501 reporters (E^2GFP, DeGFP4 and Cl-sensor). Each of these reporters was able to detect
502 pH shifts accompanying short network events on the order of 1-3 s and all three
503 reporters revealed differences in the pH responses of astrocytes and neurons over this
504 timescale. Consistent with previous work (Raimondo et al., 2012), we found that E^2GFP
505 provided the best signal to noise characteristics, although the optimal use of this
506 reporter required correction for potential fluctuations in laser output (see Materials and
507 Methods). DeGFP4 may offer greater utility for imaging in thick tissue, as it can be
508 employed with two-photon excitation. Meanwhile, our use of Cl-sensor proved an
509 excellent pH reporter within the context of a 0 Cl^- model of epilepsy, but this reporter's
510 dual sensitivity to Cl^- and pH means that it is likely to have limited use beyond this
511 particular seizure model.
512
513 Our use of organotypic hippocampal slice cultures allowed us to transfect low numbers
514 of cells with genetically-encoded reporters and afforded good optical access for pH
515 imaging from morphologically identifiable cell types. Whilst many aspects of organotypic
516 hippocampal slice cultures have been shown to resemble the *in vivo* state (De Simoni et
517 al., 2003), excitatory neurons in this experimental system are known to exhibit
518 increased axonal sprouting, which is likely to facilitate epileptiform activity (Dyhrfjeld-
519 Johnsen et al., 2010). The use of organotypic slices also meant that the astrocyte

population consisted of both protoplasmic astrocytes and reactive astrocytes, which is likely to be related to the trauma associated with the slicing procedure (Benediktsson et al., 2005). Importantly, we observed intracellular alkalinization in all astrocytic morphologies during SLEs, suggesting that the alkalinization is a general feature of astrocytes. Future work could consider using morphological criteria to sub-classify astrocytes and explore whether there are more subtle differences in pH dynamics.

Previous work has shown that membrane depolarization or electrical stimulation results in the intracellular acidification of neurons (Ahmed and Connor, 1980; Trapp et al., 1996; Zhan et al., 1998). The underlying mechanisms for this acidification are thought to include the action of Ca^{2+}/H^{+} ATPases located in the plasma membrane and endoplasmic reticulum (Makani and Chesler, 2010; Schwiening et al., 1993), the production of metabolic acids (Wang et al., 1994), and HCO_3^- efflux via activated $GABA_A$Rs (Pasternack et al., 1993; Trapp et al., 1996). Meanwhile, previous research has shown that membrane depolarization in astrocytes results in intracellular alkalinization (Boyarsky et al., 1988b, 1993; Chesler and Kraig, 1989) via the action of the electrogenic Na^+ coupled HCO_3^- transporter (NBCe1) (Bevensee, 1997; Boyarsky et al., 1993; Brookes and Turner, 1994). Here we have extended these observations by confirming the prediction that astrocytes exhibit opposing pH shifts to neurons during epileptiform activity. We demonstrate that electrogenic Na^+/HCO_3^- cotransport likely underlies SLE-associated astrocytic alkalinization, which is consistent with our observation that astrocytic alkalinization correlates closely with astrocytic membrane potential changes. This is consistent with evidence that NBCe1 is more highly

543 expressed in astrocytes than neurons (Giffard et al., 2000; Schmitt et al., 2000;
544 Theparambil et al., 2014), including recent work showing that RNA for SLC4a4 (the
545 gene encoding NBCe1) is over 20 times more highly transcribed in astrocytes (Zhang et
546 al., 2014). Nevertheless, we cannot exclude the possibility that, in addition to the
547 Na^+/HCO_3^- cotransporter, other mechanisms contribute to the intracellular pH dynamics
548 in astrocytes during seizures.
549
550 A key point from our study is that during epileptiform activity, astrocytic pH remains
551 tightly coupled to cellular activity (both astrocytic and neuronal) at the population level.
552 Indeed, astrocytic pH dynamics are more closely related to network activity than are
553 neuronal pH dynamics. This tight coupling could enable astrocytes to rapidly respond to
554 the ionic and metabolic demands of the network. For example, the coupling of astrocytic
555 alkalinization to epileptiform activity would be predicted to enhance gap junction
556 coupling between astrocytes (Spray et al., 1981), which in turn would improve the
557 spatial buffering of extracellular K^+ that accumulates during seizures (Dreier and
558 Heinemann, 1991; Wallraff et al., 2006). With regards to neurometabolic coupling,
559 Ruminot et al., (2011b) have demonstrated that alkaline transients in astrocytes are
560 sufficient to accelerate glycolysis and lactate production (Bittner et al., 2011), which is
561 subsequently transported via the lactate shuttle to neurons. In conjunction with our
562 observations, this would suggest that rapid, activity-dependent alkaline intracellular pH
563 transients could provide a dynamic mechanism for astrocytes to anticipate neuronal
564 demand for metabolic substrates in the face of enhanced network activity (Barros,
565 2013). This may be particularly relevant in the context of epileptic seizures where

566 neuronal metabolic demand is markedly increased. Indeed, it is possible that such a
567 mechanism could enable astrocytes to help maintain epileptiform activity by ensuring
568 that the energy demands of nearby neurons remain met (Gómez-Gonzalo et al., 2010).
569
570 More generally, our results support the view that the central nervous system exhibits
571 compartment-specific changes in pH during seizure activity. Intracellular pH changes
572 are largely the result of H^+ equivalents moving across the cell membrane, which will
573 therefore manifest as pH changes in the extracellular space. Our observations of
574 different seizure-associated pH response kinetics in the two major intracellular
575 compartments, astrocytes and neurons, is consistent with reports of complex pH
576 transients in the extracellular space (Caspers and Speckmann, 1972; Urbanics et al.,
577 1978; Xiong and Stringer, 2000). Rapid astrocytic alkalinization during seizure activity
578 would be predicted to result in an early extracellular acidification, which would precede
579 or reduce the extracellular alkalosis generated by intraneuronal acidification. Indeed,
580 previous work has observed such an effect in the hippocampus and in a manner that
581 correlates with the maturation of astrocytes (Xiong and Stringer, 2000). Astrocytic
582 acidification of the extracellular space has long been postulated as a mechanism for
583 modulating network excitability (Chesler, 2003; Deitmer and Rose, 1996; Ransom,
584 2000), perhaps through pH-dependent effects on synaptic transmission and/or voltage-
585 gated channels (Barnes and Bui, 1991; Pasternack et al., 1996; Tang et al., 1990). How
586 more complex extracellular pH transients might modulate synaptic transmission and
587 evolving seizure activity remains an important question for the future.
588

589 In summary, our findings support the idea that astrocytes are uniquely positioned to
590 regulate network activity under physiological and pathophysiological conditions.
591 Differences in cell-specific pH regulatory mechanisms mean that during epileptiform
592 activity, astrocytes experience pH changes that are highly distinct from nearby neurons,
593 both in terms of their direction and temporal kinetics. This work adds further impetus to
594 examine the role of astrocytes in controlling the spread of epileptiform activity (Bedner
595 et al., 2015; Gómez-Gonzalo et al., 2010).
596

Figure Legends

Figure 1: Astrocytes experience rapid intracellular alkalinization during epileptiform activity

(A) Schematic (left) showing the experimental setup in which a hippocampal pyramidal neuron expressing a genetically-encoded pH reporter was imaged, whilst a simultaneous patch clamp recording was performed from a neighboring neuron. Dynamic intracellular pH measurements from a representative CA3 pyramidal neuron expressing E^2GFP (right, blue trace) and current clamp recording from a neighboring pyramidal neuron (black trace, somata <200 µm apart), which provided a readout of the epileptiform activity in Mg^{2+}-free ACSF. Acidic intracellular pH shifts were closely associated with SLEs (onset indicated by vertical dashed lines). (B) Schematic (left) showing a similar setup as in 'A' for the measurement of pH dynamics in hippocampal astrocytes during SLEs. Intracellular pH measurements made from a representative astrocyte expressing E^2GFP (right, red trace, same astrocyte as in 'C') and current clamp recording from a neighboring pyramidal neuron (black trace), which provided a readout of the epileptiform activity in Mg^{2+}-free ACSF. Individual SLEs of different durations are closely associated with rapid intracellular alkaline transients in the astrocyte. (C) Confocal image (top) of an astrocyte expressing E^2GFP. After performing pH imaging (shown in 'B'), this astrocyte was targeted for whole cell patch clamp recording and confirmed to exhibit a low membrane resistance (Rm = 20.5 MΩ) and lack voltage-gated conductances in response to current injection (inset). Confocal image (bottom) of a neuron expressing E^2GFP, which exhibited action potentials in

response to current injection (inset). (D) Population data demonstrating a significant difference in pre-SLE intracellular pH between hippocampal neurons and astrocytes. *** $P < 0.0001$, *t* test. (E) Population data showing the peak shift in intracellular pH as a function of the duration of the epileptiform activity (data from 23 neurons, blue, and 24 astrocytes, red). For neurons, the peak change in pH was negatively correlated with the duration of the SLE ($r = -0.6719$, $P < 0.0001$, Pearson correlation). For astrocytes, the peak pH shift was positively correlated with the length of the SLE ($r = 0.5766$, $P < 0.0001$, Pearson correlation).

Figure 2: Multiple genetically-encoded pH sensors reveal astrocytic alkalinization during epileptiform activity

(A) Calibration curve relating the fluorescence ratio of DeGFP4-expressing cells to their intracellular pH. This revealed the reporter to have a pKa of 7.4. Similarly, calibration of E^2GFP (B) and Cl-sensor (C) revealed a pKa of 7.5 and 7.7 for these genetically-encoded pH sensors, respectively. (D) An astrocyte expressing the pH sensor DeGFP4 was imaged for pH (red trace), whilst 0 Mg^{2+} induced epileptiform activity was monitored via a simultaneous current clamp recording from a nearby pyramidal neuron (black trace). Epileptiform activity was associated with a pronounced increase in the astrocyte's pH. (E) pH imaging from an astrocyte expressing the pH sensor E^2GFP revealed intracellular alkalinization (red trace) during periods of epileptiform activity induced with 0 Cl^- ACSF (black trace). (F) pH imaging from an astrocyte expressing the

pH-sensitive Cl-sensor also reveals intracellular alkalinization (red trace) during periods of epileptiform activity induced with 0 Cl^- ACSF (black trace).

Figure 3: Cell-type specific changes in pH during epileptiform activity

(A) Astrocytes (red) and neurons (blue) imaged with the pH sensor E^2GFP, showed opposing pH transients during 0 Mg2+ induced SLEs (20-40 s duration). Neurons exhibited transient acidic shifts, whereas astrocytes exhibited transient alkaline shifts during periods of epileptiform activity. Similar differences were observed when intracellular pH was imaged with E^2GFP during 0 Cl^- induced SLEs (B), or DeGFP4 during 0 Mg^{2+} induced SLEs (C), or Cl-sensor during 0 Cl^- induced SLEs (D). *** $P <$ 0.0001, *t* test.

Figure 4: Alkaline transients in astrocytes during epileptiform activity are mediated by depolarization and the sodium-bicarbonate co-transporter NBCe1

(A) Dual whole cell current clamp recording from a pair of CA3 pyramidal neurons (somata <200 µm apart) during 0 Mg^{2+} induced epileptiform activity. Dashed line indicates onset of a SLE. The membrane potential of the two neurons was highly synchronous, as indicated by the tight correlation in the cells' membrane potentials (r = 0.92, Pearson correlation). Action potential generation in response to somatic current injection (insets) confirmed both cells were neuronal. (B) Dual whole cell current clamp recording from a pyramidal neuron (black trace) and a nearby astrocyte (red trace;

somata <200 µm apart). Note that the astrocytic membrane potential depolarization during the SLE is tightly correlated with neuronal membrane potential (r = 0.82, Pearson correlation). Response to somatic current injection confirmed the identity of the cells (insets). (C) Population data revealed a high correlation in the membrane potential between pyramidal neurons (r = 0.91 ± 0.01, Pearson correlation), and between pyramidal neurons and astrocytes (r = 0.80 ± 0.02, Pearson correlation) during SLEs. (D) Under control conditions intracellular pH imaging with E^2GFP (red trace) revealed transient alkalinizations that were associated with 0 Mg^{2+} induced epileptiform activity, as monitored from a nearby pyramidal neuron (black trace). (E) Bath application of the selective Na^+ / HCO_3^- cotransporter blocker S0859 (50 µM) to the same cells as in 'D', resulted in a marked attenuation of the astrocytic alkalinizations. (F) Population data demonstrate that S0859 blocks the astrocytic alkalinizations and eliminates the correlation between SLE duration and the size of the alkaline shift (r = 0.4289, P = 0.08 vs. r = 0.69, P < 0.0001, Pearson correlation). (G) For SLEs of comparable duration (< 35 s duration), S0859 significantly reduced the peak change in astrocytic pH_i associated with 0 Mg^{2+}-induced SLEs (left) and 0 Cl^--induced SLEs (center). Low HCO_3^- ACSF also reduced SLE-associated astrocytic alkaline shifts in 0 Cl^- ACSF (right). * P < 0.05, ** P < 0.01, *** P < 0.0001, t test.

Figure 5: The kinetics of pH transients differ between astrocytes and neurons during epileptiform activity

687 (A) A confocal image of a CA3 pyramidal neuron and neighboring astrocyte both
688 expressing E^2GFP. The expanded region shows a magnified view of the astrocyte and
689 adjacent apical dendrite of the pyramidal neuron. Dashed boxes indicate regions of
690 interest used for pH measurements. (B) Current clamp recording of a nearby neuron
691 (somata <200 µm apart) provides a readout of 0 Mg^{2+} induced epileptiform activity
692 (black trace). Simultaneous pH imaging from the regions of interest indicated by the
693 dashed lines in 'A'. The astrocyte (red) exhibited a transient increase in pH that was
694 closely aligned with the SLE (grey bar), whilst the neuron (blue) exhibited a more
695 prolonged decrease in pH. The arrowheads indicate the point of maximal pH shift (filled
696 arrowheads) and the point at which pH recovered to baseline (empty arrowheads). (C)
697 Representative changes in intracellular pH during 0 Mg^{2+} induced epileptiform activity in
698 an astrocyte (red traces) and a CA3 pyramidal neuron (blue traces) within the same
699 hippocampal slice. The astrocyte exhibited a more rapid alkalinization, which peaked
700 and then recovered more quickly than the more sustained acidification of the neuron.
701 (D) Similar differences in the kinetics of cell-specific pH shifts were observed when
702 epileptiform activity was induced with 0 Cl^- ACSF. (E) Population data show that
703 astrocytes reached their peak pH shift significantly faster than neurons in both 0 Mg^{2+}
704 and 0 Cl^- induced epileptiform activity. (F) The time for pH to recover to baseline was
705 also significantly faster in astrocytes than neurons in both 0 Mg^{2+} and 0 Cl^- induced
706 epileptiform activity. *** $P < 0.0001$, *t* test.
707

Figure 6: Simultaneous recordings from different cell-pair combinations reveal that astrocytic pH dynamics closely reflect both astrocytic and neuronal membrane potential dynamics

(A) Paired pH imaging (green trace) and whole cell patch clamp recording (black trace) from a pair of astrocytes in stratum radiatum of CA3 revealed a close correlation between changes in astrocytic pH and changes in astrocytic membrane potential during epileptiform activity (r = 0.72, Pearson correlation). (B) A similar experiment on an astrocyte-neuron pair also revealed a high degree of correlation between changes in astrocytic pH and neuronal membrane potential (r = 0.49, Pearson correlation). (C) In contrast, a similar experiment on a neuron-neuron pair revealed a much lower correlation between the change in neuronal pH and the change in neuronal membrane potential (r = 0.17, Pearson correlation).

Figure 7: Astrocytic pH dynamics are more strongly coupled to network activity than neuronal pH dynamics

(A) The absolute correlation between astrocytic pH and astrocytic membrane potential was highest (r = 0.71 ± 0.02), followed by the correlation between astrocytic pH and neuronal membrane potential (r = 0.43 ± 0.04), and the weakest correlation was observed between neuronal –pH and neuronal membrane potential (r = 0.15 ± 0.05). (B) Cross correlation analysis demonstrated that the maximum correlation between traces was observed when pH measurements were shifted with a negative lag, consistent with pH changes occurring in response to network activity. Shaded regions depict SEM. (C)

The highest cross correlation values (calculated after shifting pH relative to membrane potential, as in 'B') were observed between astrocytic pH and astrocytic membrane potential (r = 0.77 ± 0.02). The next highest cross correlation values were observed between astrocytic pH and neuronal membrane potential (r = 0.68 ± 0.02). These correlation values were both significantly greater than the cross correlation values observed between neuronal –pH and neuronal membrane potential (r = 0.45 ± 0.04). * P < 0.05, *** P < 0.0001, t test.

References

Ahmed, Z., and Connor, J. A. (1980). Intracellular pH changes induced by calcium influx during electrical activity in molluscan neurons. *J. Gen. Physiol.* 75, 403–426. doi:10.1085/jgp.75.4.403.

Anderson, W. W., Lewis, D. V, Swartzwelder, H. S., and Wilson, W. A. (1986). Magnesium-free medium activates seizure-like events in the rat hippocampal slice. *Brain Res.* 398, 215–9.

Araque, A., Parpura, V., Sanzgiri, R. P., and Haydon, P. G. (1999). Tripartite synapses: glia, the unacknowledged partner. *Trends Neurosci.* 22, 208–215. doi:10.1016/S0166-2236(98)01349-6.

Arosio, D., Ricci, F., Marchetti, L., Gualdani, R., Albertazzi, L., and Beltram, F. (2010). Simultaneous intracellular chloride and pH measurements using a GFP-based sensor. *Nat. Methods* 7, 516–8. doi:10.1038/nmeth.1471.

Barnes, S., and Bui, Q. (1991). Modulation of calcium-activated chloride current via pH-induced changes of calcium channel properties in cone photoreceptors. *J. Neurosci.* 11, 4015–4023.

754 Barros, L. F. (2013). Metabolic signaling by lactate in the brain. *Trends Neurosci.*, 1–9.
755 doi:10.1016/j.tins.2013.04.002.
756 Bedner, P., Dupper, a., Huttmann, K., Muller, J., Herde, M. K., Dublin, P., et al. (2015).
757 Astrocyte uncoupling as a cause of human temporal lobe epilepsy. *Brain*, 1–15.
758 doi:10.1093/brain/awv067.
759 Benediktsson, A. M., Schachtele, S. J., Green, S. H., and Dailey, M. E. (2005). Ballistic
760 labeling and dynamic imaging of astrocytes in organotypic hippocampal slice
761 cultures. *J. Neurosci. Methods.* 141, 41–53. doi:10.1016/j.jneumeth.2004.05.013.
762 Bevensee, M. O. (1997). Intracellular pH Regulation in Cultured Astrocytes from Rat
763 Hippocampus . I. Role of HCO3-. *J. Gen. Physiol.* 110, 453–465.
764 doi:10.1085/jgp.110.4.453.
765 Bittner, C. X., Valdebenito, R., Ruminot, I., Loaiza, A., Larenas, V., Sotelo-Hitschfeld, T.,
766 et al. (2011). Fast and reversible stimulation of astrocytic glycolysis by K+ and a
767 delayed and persistent effect of glutamate. *J. Neurosci.* 31, 4709–13.
768 doi:10.1523/JNEUROSCI.5311-10.2011.
769 Bizzarri, R., Serresi, M., Luin, S., and Beltram, F. (2009). Green fluorescent protein
770 based pH indicators for in vivo use: a review. *Anal. Bioanal. Chem.* 393, 1107–
771 1122. doi:10.1007/s00216-008-2515-9.
772 Boyarsky, G., Ganz, M. B., Sterzel, R. B., and Boron, W. F. (1988a). pH regulation in
773 single glomerular mesangial cells. I. Acid extrusion in absence and presence of
774 HCO3-. *Am. J. Physiol.* 255, 844–56.
775 Boyarsky, G., Ransom, B., Carlini, W., and Boron, W. (1988b). Intracellular pH
776 regulation in cultured mammalian astrocytes. *Soc. Neurosci. Abstr.*

777 Boyarsky, G., Ransom, B., Schlue, W. R., Davis, M. B., and Boron, W. F. (1993).
778 Intracellular pH regulation in single cultured astrocytes from rat forebrain. *Glia* 8,
779 241–8. doi:10.1002/glia.440080404.
780 Brookes, N., and Turner, R. J. (1994). K(+)-induced alkalinization in mouse cerebral
781 astrocytes mediated by reversal of electrogenic Na(+)-HCO3- cotransport. *Am. J.*
782 *Physiol.* 267, C1633–40.
783 Caspers, H., and Speckmann, E. . (1972). Cerebral pO2, pCO2 and pH: changes during
784 convulsive activity and their significance for spontaneous arrest of seizures.
785 *Epilepsia*, 699–725.
786 Ch'en, F. F.-T., Villafuerte, F. C., Swietach, P., Cobden, P. M., and Vaughan-Jones, R.
787 D. (2008). S0859, an N-cyanosulphonamide inhibitor of sodium-bicarbonate
788 cotransport in the heart. *Br. J. Pharmacol.* 153, 972–82.
789 doi:10.1038/sj.bjp.0707667.
790 Chesler, M. (2003). Regulation and modulation of pH in the brain. *Physiol. Rev.* 83,
791 1183–221. doi:10.1152/physrev.00010.2003.
792 Chesler, M., and Kraig, R. (1989). Intracellular pH transients of mammalian astrocytes.
793 *J. Neurosci.* 9, 2011–9.
794 Choi, H. B., Gordon, G. R. J., Zhou, N., Tai, C., Rungta, R. L., Martinez, J., et al. (2012).
795 Metabolic Communication between Astrocytes and Neurons via Bicarbonate-
796 Responsive Soluble Adenylyl Cyclase. *Neuron* 75, 1094–1104.
797 doi:10.1016/j.neuron.2012.08.032.
798 Deitmer, J. W., and Rose, C. R. (1996). pH regulation and proton signalling by glial
799 cells. *Prog. Neurobiol.* 48, 73–103. doi:10.1016/0301-0082(95)00039-9.

800 Deitmer, J. W., and Szatkowski, M. (1990). Membrane potential dependence of
801 intracellular pH regulation by identified glial cells in the leech central nervous
802 system. *J. Physiol.* 421, 617–631.
803 Dreier, J., and Heinemann, U. (1991). Regional and time dependent variations of low
804 Mg2+ induced epileptiform activity in rat temporal cortex slices. *Exp. Brain Res.* 3,
805 581–596.
806 Dyhrfjeld-Johnsen, J., Berdichevsky, Y., Swiercz, W., Sabolek, H., and Staley, K. J.
807 (2010). Interictal spikes precede ictal discharges in an organotypic hippocampal
808 slice culture model of epileptogenesis. *J. Clin. Neurophysiol.* 27, 418–24.
809 doi:10.1097/WNP.0b013e3181fe0709.
810 Ellender, T. J., Raimondo, J. V., Irkle, a., Lamsa, K. P., and Akerman, C. J. (2014).
811 Excitatory Effects of Parvalbumin-Expressing Interneurons Maintain Hippocampal
812 Epileptiform Activity via Synchronous Afterdischarges. *J. Neurosci.* 34, 15208–
813 15222. doi:10.1523/JNEUROSCI.1747-14.2014.
814 Erecińska, M., Deas, J., and Silver, I. A. (1995). The effect of pH on glycolysis and
815 phosphofructokinase activity in cultured cells and synaptosomes. *J. Neurochem.*
816 65, 2765–2772.
817 Giffard, R. G., Papadopoulos, M. C., van Hooft, J. a, Xu, L., Giuffrida, R., and Monyer,
818 H. (2000). The electrogenic sodium bicarbonate cotransporter: developmental
819 expression in rat brain and possible role in acid vulnerability. *J. Neurosci.* 20, 1001–
820 8.
821 Gómez-Gonzalo, M., Losi, G., Chiavegato, A., Zonta, M., Cammarota, M., Brondi, M., et
822 al. (2010). An excitatory loop with astrocytes contributes to drive neurons to seizure

threshold. *PLoS Biol.* 8, e1000352. doi:10.1371/journal.pbio.1000352.

Grynkiewicz, G., Poenie, M., and Tsien, R. Y. (1985). A new generation of Ca2+ indicators with greatly improved fluorescence properties. *J. Biol. Chem* 260, 3440–50.

Hinterkeuser, S., Schröder, W., Hager, G., Seifert, G., Blümcke, I., Elger, C. E., et al. (2000). Astrocytes in the hippocampus of patients with temporal lobe epilepsy display changes in potassium conductances. *Eur. J. Neurosci.* 12, 2087–96.

Howarth, C., Gleeson, P., and Attwell, D. (2012). Updated energy budgets for neural computation in the neocortex and cerebellum. *J. Cereb. Blood Flow Metab.* 32, 1222–32. doi:10.1038/jcbfm.2012.35.

Majumdar, D., and Bevensee, M. O. (2010). Na-coupled bicarbonate transporters of the solute carrier 4 family in the nervous system: function, localization, and relevance to neurologic function. *Neuroscience* 171, 951–72. doi:10.1016/j.neuroscience.2010.09.037.

Makani, S., and Chesler, M. (2010). Rapid rise of extracellular pH evoked by neural activity is generated by the plasma membrane calcium ATPase. *J. Neurophysiol.* 103, 667–76. doi:10.1152/jn.00948.2009.

Markova, O., Mukhtarov, M., Real, E., Jacob, Y., and Bregestovski, P. (2008). Genetically encoded chloride indicator with improved sensitivity. *J. Neurosci. Meth.* 170, 67–76. doi:10.1016/j.jneumeth.2007.12.016.

McKhann, G. M., D'Ambrosio, R., and Janigro, D. (1997). Heterogeneity of astrocyte resting membrane potentials and intercellular coupling revealed by whole-cell and gramicidin-perforated patch recordings from cultured neocortical and hippocampal

slice astrocytes. *J. Neurosci.* 17, 6850–63.

O'Connor, E., Sontheimer, H., and Ransom, B. (1994). Rat hippocampal astrocytes exhibit electrogenic sodium-bicarbonate co-transport. *J. Neurophysiol.* 72, 2580–2589.

Pappas, C. A., and Ransom, B. R. (1994). Depolarization-induced alkalinization (DIA) in rat hippocampal astrocytes. *J. Neurophysiol.* 72, 2816–26.

Pasternack, M., Smirnov, S., and Kaila, K. (1996). Proton Modulation of Functionally Distinct GABAA Receptors in Acutely Isolated Pyramidal Neurons of Rat Hippocampus. *Neuropharmacology* 35, 1279–1288. doi:10.1016/S0028-3908(96)00075-5.

Pasternack, M., Voipio, J., and Kaila, K. (1993). Intracellular carbonic anhydrase activity and its role in GABA-induced acidosis in isolated rat hippocampal pyramidal neurones. *Acta Physiol. Scand.* 148, 229–231.

Pellerin, L., and Magistretti, P. J. (1994). Glutamate Uptake into Astrocytes Stimulates Aerobic Glycolysis: A Mechanism Coupling Neuronal Activity to Glucose Utilization. *Proc Natl Acad Sci U S A.* 91, 10625–10629. doi:10.1073/pnas.91.22.10625.

Raimondo, J. V, Joyce, B., Kay, L., Schlagheck, T., Newey, S. E., Srinivas, S., et al. (2013). A genetically-encoded chloride and pH sensor for dissociating ion dynamics in the nervous system. *Front. Cell. Neurosci.* 7, 202. doi:10.3389/fncel.2013.00202.

Raimondo, J. V., Burman, R. J., Katz, A. a., and Akerman, C. J. (2015). Ion dynamics during seizures. *Front. Cell. Neurosci.* 9, 1–14. doi:10.3389/fncel.2015.00419.

Raimondo, J. V., Irkle, A., Wefelmeyer, W., Newey, S. E., and Akerman, C. J. (2012). Genetically encoded proton sensors reveal activity-dependent pH changes in

neurons. *Front. Mol. Neurosci.* 5, 1–12. doi:10.3389/fnmol.2012.00068.

Ransom, B. R. (2000). Glial modulation of neural excitability mediated by extracellular pH: a hypothesis revisited. *Prog. Brain Res.* 125, 217–228.

Rose, C. R., and Deitmer, J. W. (1995). Stimulus-evoked changes of extra- and intracellular pH in the leech central nervous system. II. Mechanisms and maintenance of pH homeostasis. *J. Neurophysiol.* 73, 132–140.

Ruminot, I., Gutiérrez, R., Peña-Münzenmayer, G., Añazco, C., Sotelo-Hitschfeld, T., Lerchundi, R., et al. (2011a). NBCe1 mediates the acute stimulation of astrocytic glycolysis by extracellular K+. *J. Neurosci.* 31, 14264–71. doi:10.1523/JNEUROSCI.2310-11.2011.

Ruminot, I., Gutiérrez, R., Peña-Münzenmayer, G., Añazco, C., Sotelo-Hitschfeld, T., Lerchundi, R., et al. (2011b). NBCe1 mediates the acute stimulation of astrocytic glycolysis by extracellular K+. *J. Neurosci.* 31, 14264–71. doi:10.1523/JNEUROSCI.2310-11.2011.

Schmitt, B. M., Berger, U. V, Douglas, R. M., Bevensee, M. O., Hediger, M. a, Haddad, G. G., et al. (2000). Na/HCO3 cotransporters in rat brain: expression in glia, neurons, and choroid plexus. *J. Neurosci.* 20, 6839–48.

Schwiening, C. J., Kennedy, H. J., and Thomas, R. C. (1993). Calcium-hydrogen exchange by the plasma membrane Ca-ATPase of voltage-clamped snail neurons. *Proc. Biol. Sci.* 253, 285–9.

De Simoni, A., Griesinger, C. B., and Edwards, F. A. (2003). Development of rat CA1 neurones in acute versus organotypic slices: role of experience in synaptic morphology and activity. *J. Physiol.* 550, 135–47.

doi:10.1113/jphysiol.2003.039099.

Spray, D., Harris, A., and Bennett, M. (1981). Gap junctional conductance is a simple and sensitive function of intracellular pH. *Science (80-.).* 211, 712.

Taira, T., Smirnov, S., Voipio, J., and Kaila, K. (1993). Intrinsic proton modulation of excitatory transmission in rat hippocampal slices. *Neuroreport* 4, 93.

Tang, C. M., Dichter, M., and Morad, M. (1990). Modulation of the N-Methyl-D-Aspartate Channel by Extracellular H+. *Proc. Natl. Acad. Sci. USA* 87, 6445–6449. doi:10.1073/pnas.87.16.6445.

Theparambil, S. M., Ruminot, I., Schneider, H.-P., Shull, G. E., and Deitmer, J. W. (2014). The electrogenic sodium bicarbonate cotransporter NBCe1 is a high-affinity bicarbonate carrier in cortical astrocytes. *J. Neurosci.* 34, 1148–57. doi:10.1523/JNEUROSCI.2377-13.2014.

Trapp, S., Luckermann, M., Brooks, P. A., and Ballanyi, K. (1996). Acidosis of rat dorsal vagal neurons in situ during spontaneous and evoked activity. *J. Physiol.* 496, 695–710.

Traynelis, S. F., and Cull-Candy, S. G. (1990). Proton inhibition of N-methyl-D-aspartate receptors in cerebellar neurons. *Nature* 345, 347–350. doi:10.1038/345347a0.

Urbanics, R., Leniger-Follert, E., and Lübbers, D. W. (1978). Time course of changes of extracellular H+ and K+ activities during and after direct electrical stimulation of the brain cortex. *Pflugers Arch.* 378, 47–53.

Wallraff, A., Köhling, R., Heinemann, U., Theis, M., Willecke, K., and Steinhäuser, C. (2006). The impact of astrocytic gap junctional coupling on potassium buffering in the hippocampus. *J. Neurosci.* 26, 5438–47. doi:10.1523/JNEUROSCI.0037-

915 06.2006.
916 Walz, W. (2000). Role of astrocytes in the clearance of excess extracellular potassium.
917 *Neurochem. Int.* 36, 291–300.
918 Wang, G. J., Randall, R. D., and Thayer, S. A. (1994). Glutamate-induced intracellular
919 acidification of cultured hippocampal neurons demonstrates altered energy
920 metabolism resulting from Ca2+ loads. *J. Neurophysiol.* 72, 2563–2569.
921 Xiong, Z. Q., Saggau, P., and Stringer, J. L. (2000). Activity-dependent intracellular
922 acidification correlates with the duration of seizure activity. *J. Neurosci.* 20, 1290–6.
923 Xiong, Z. Q., and Stringer, J. L. (2000). Regulation of extracellular pH in the developing
924 hippocampus. *Dev. Brain Res.* 122, 113–117. doi:10.1016/S0165-3806(00)00057-
925 2.
926 Yamamoto, C. (1972). Intracellular study of seizure-like afterdischarges elicited in thin
927 hippocampal sections in vitro. *Exp. Neurol.* 35, 154–64.
928 Yamamoto, C., and Kawai, N. (1967). Seizure discharges evoked in vitro in thin section
929 from guinea pig hippocampus. *Science* 155, 341–342.
930 doi:10.1126/science.155.3760.341.
931 Zhan, R. Z., Fujiwara, N., Tanaka, E., and Shimoji, K. (1998). Intracellular acidification
932 induced by membrane depolarization in rat hippocampal slices: Roles of
933 intracellular Ca2+ and glycolysis. *Brain Res.* 780, 86–94. doi:10.1016/S0006-
934 8993(97)01149-9.
935 Zhang, Y., Chen, K., Sloan, S. A., Bennett, M. L., Scholze, A. R., O'Keeffe, S., et al.
936 (2014). An RNA-sequencing transcriptome and splicing database of glia, neurons,
937 and vascular cells of the cerebral cortex. *J. Neurosci.* 34, 11929–11947.

doi:10.1523/JNEUROSCI.1860-14.2014.

Zucker, R. M., and Price, O. (2001). Evaluation of confocal microscopy system performance. *Cytometry* 44, 273–94.

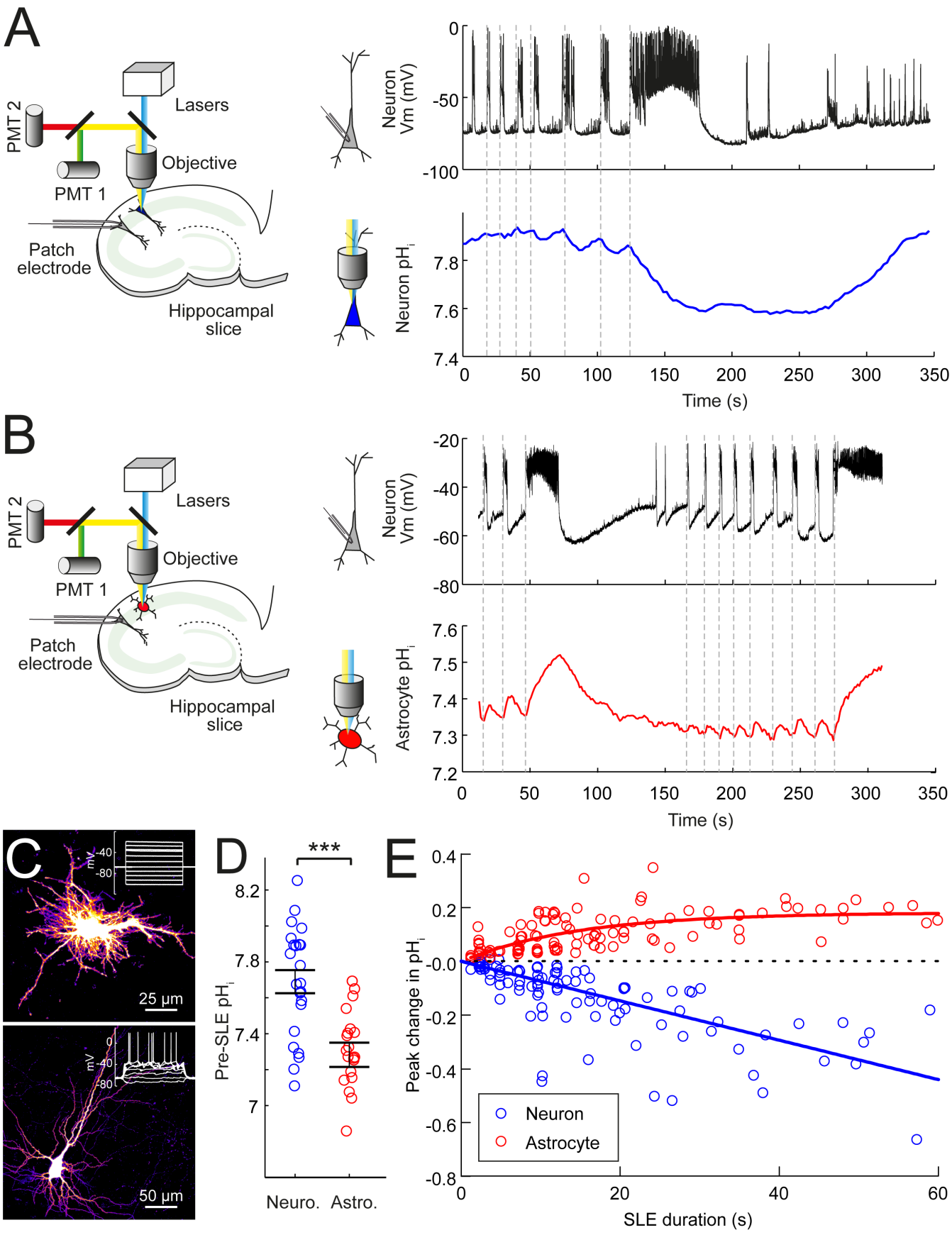

Figure 1: Astrocytes experience rapid intracellular alkalinization during epileptiform activity

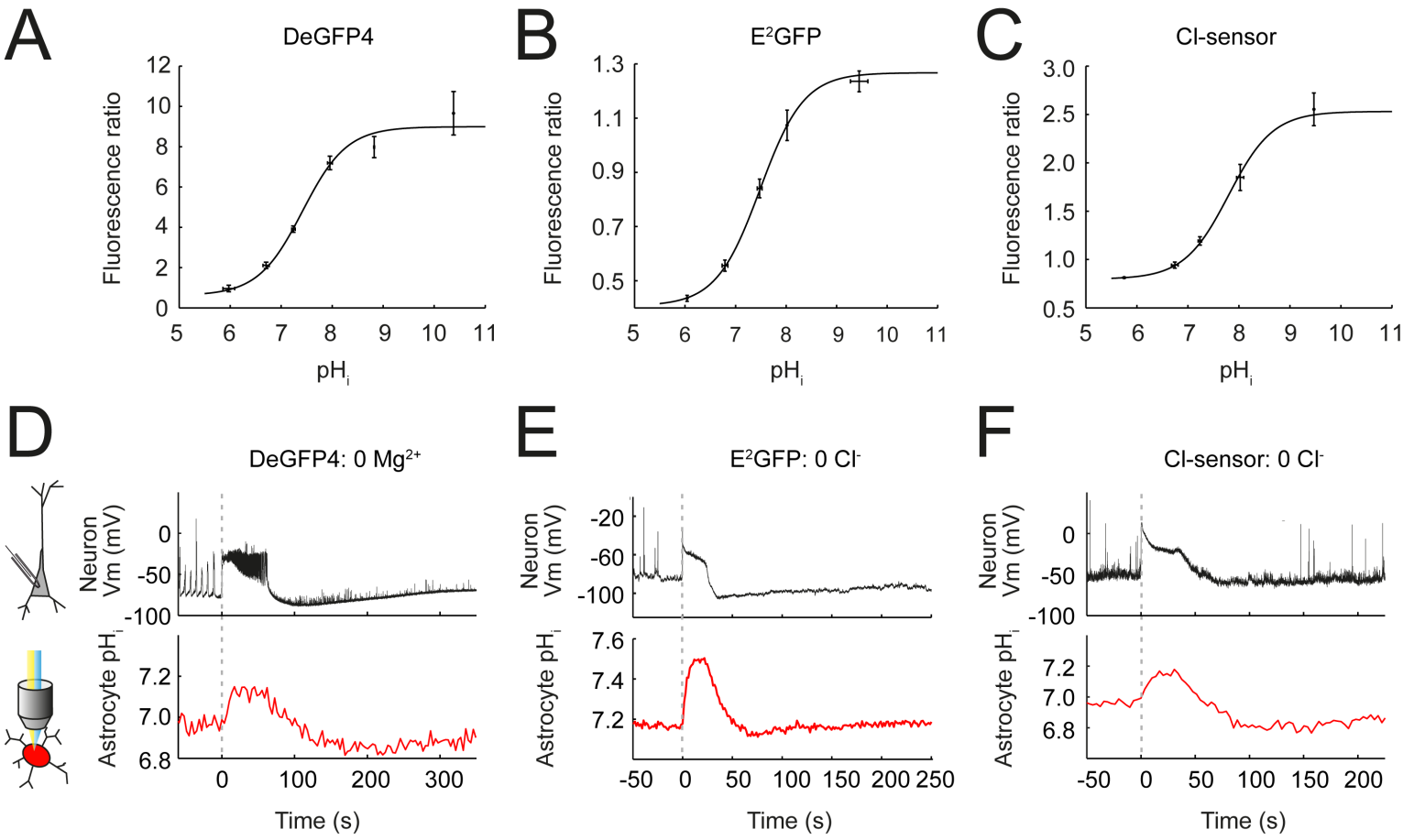

Figure 2: Multiple genetically-encoded pH sensors reveal astrocytic alkalinization during epileptiform activity

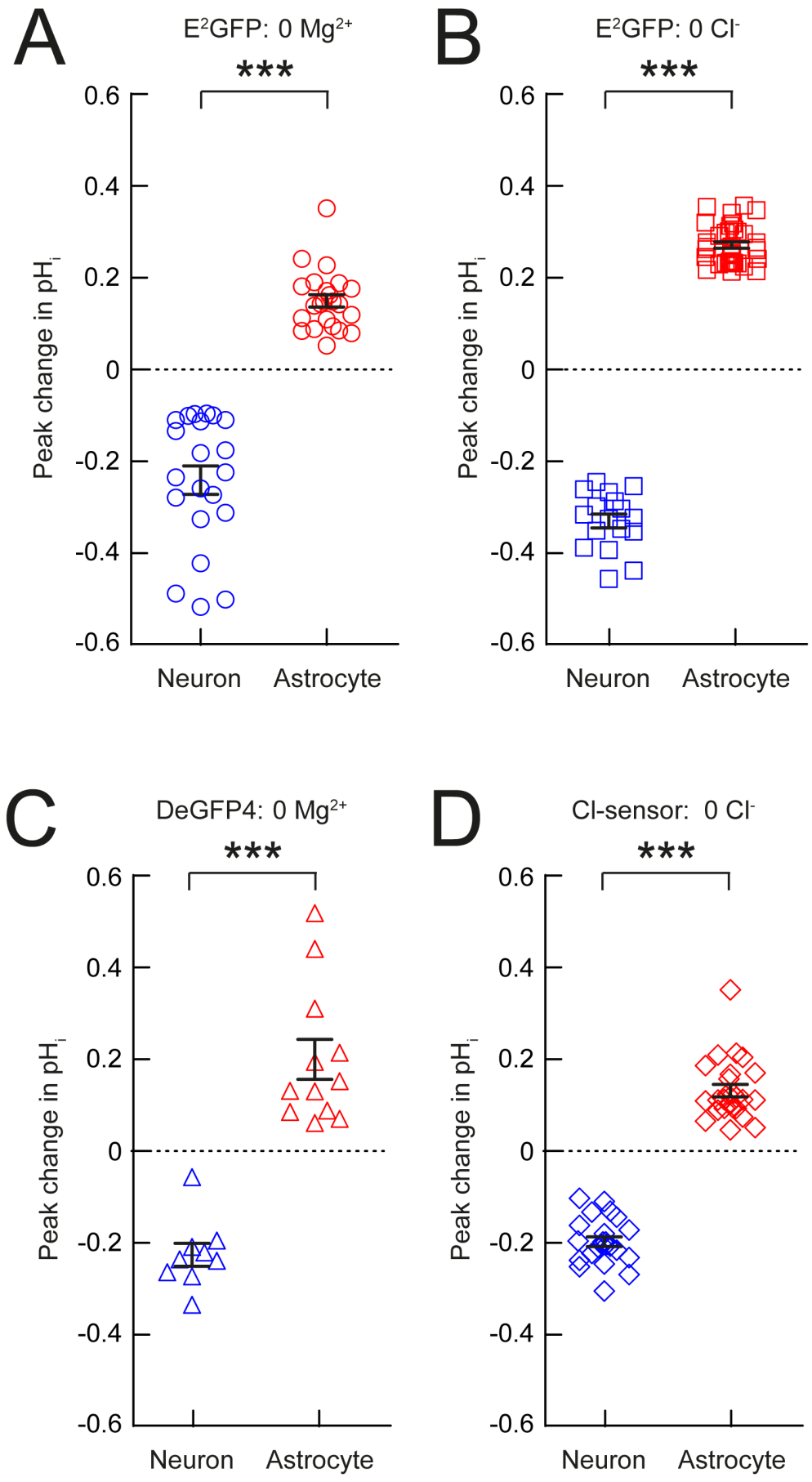

Figure 3: Cell-type specific changes in pH during epileptiform activity

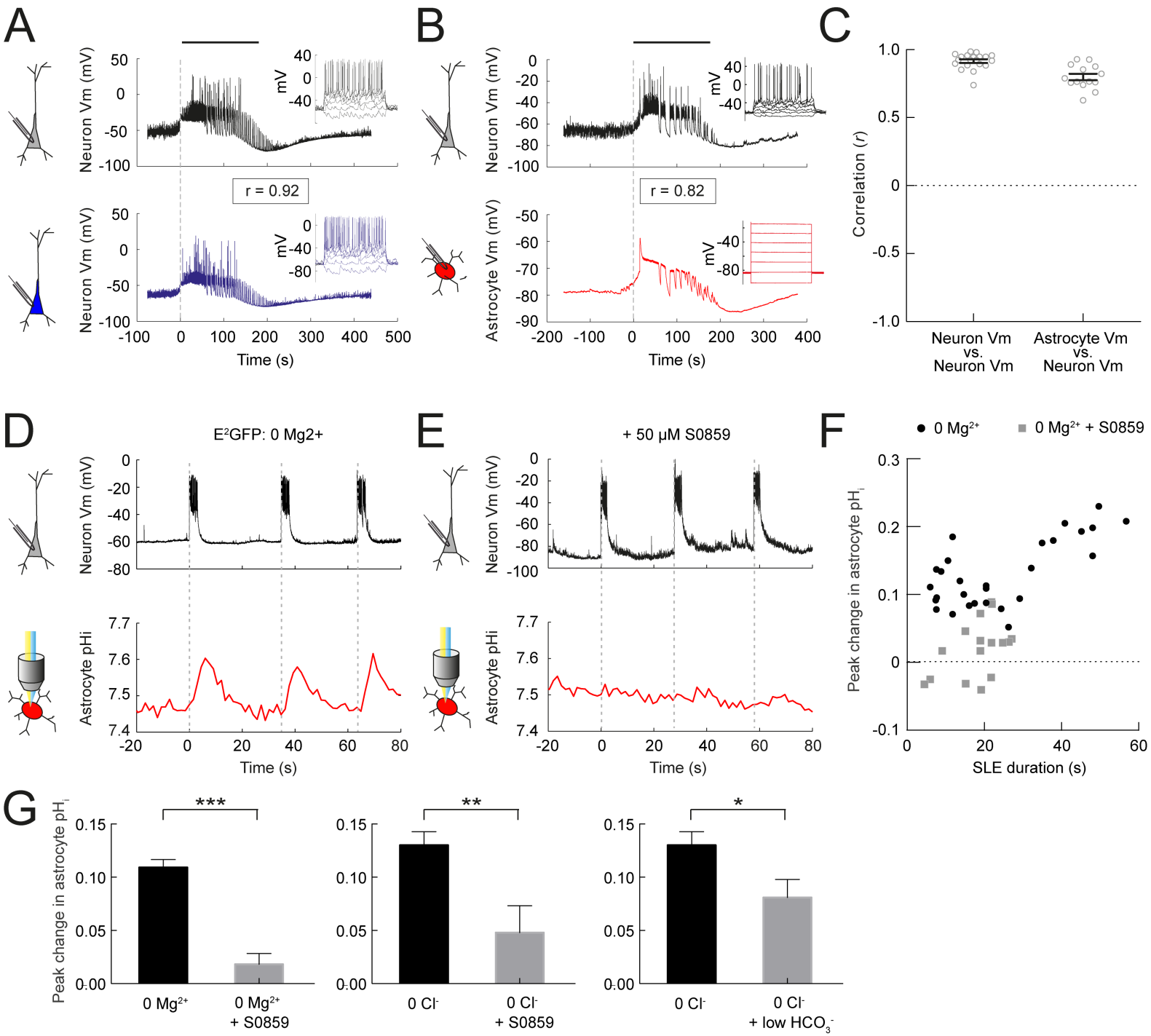

Figure 4: Alkaline transients in astrocytes during epileptiform activity are mediated by depolarization and the sodium-bicarbonate co-transporter NBCe1

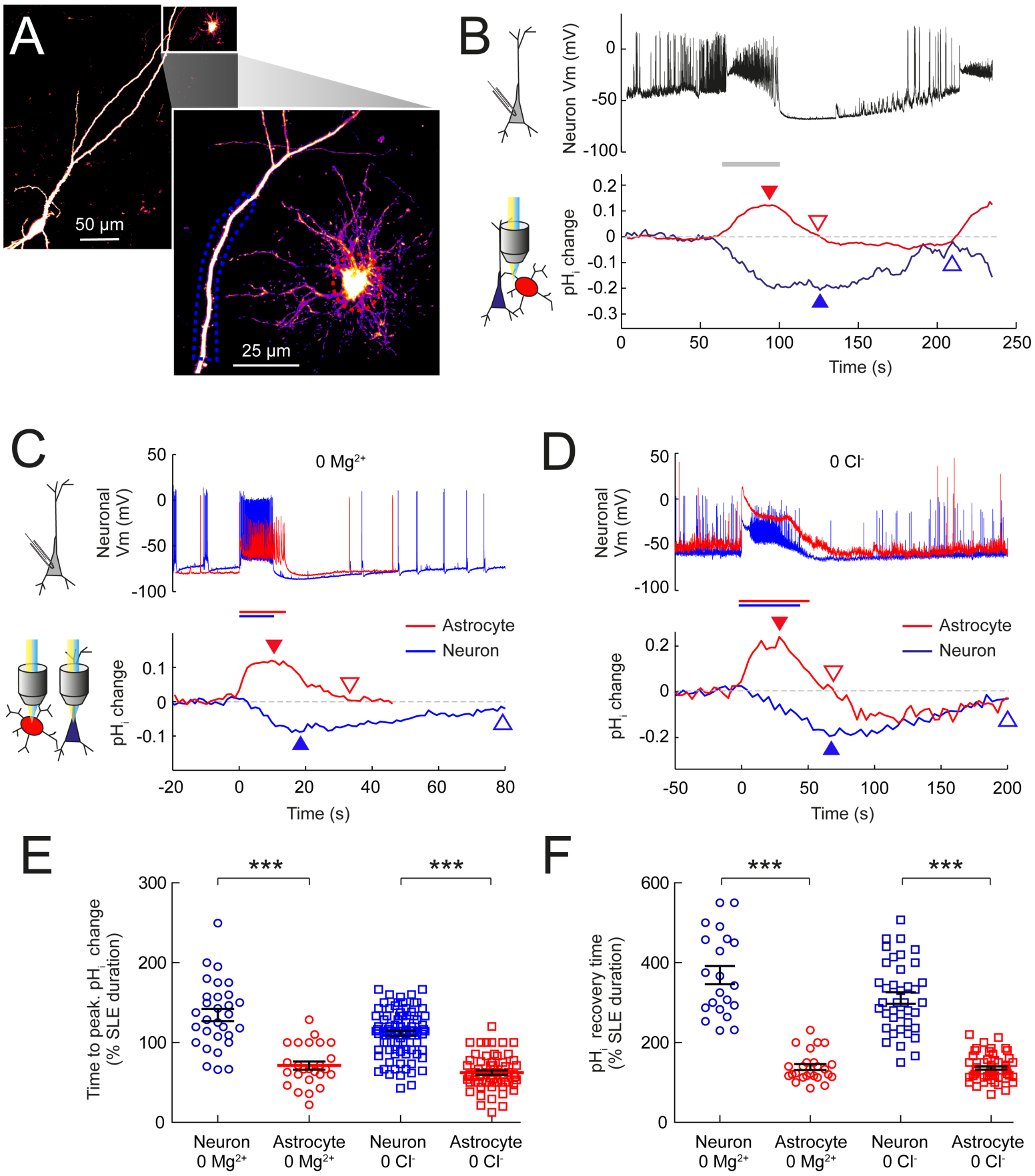

Figure 5: The kinetics of pH transients differ between astrocytes and neurons during epileptiform activity

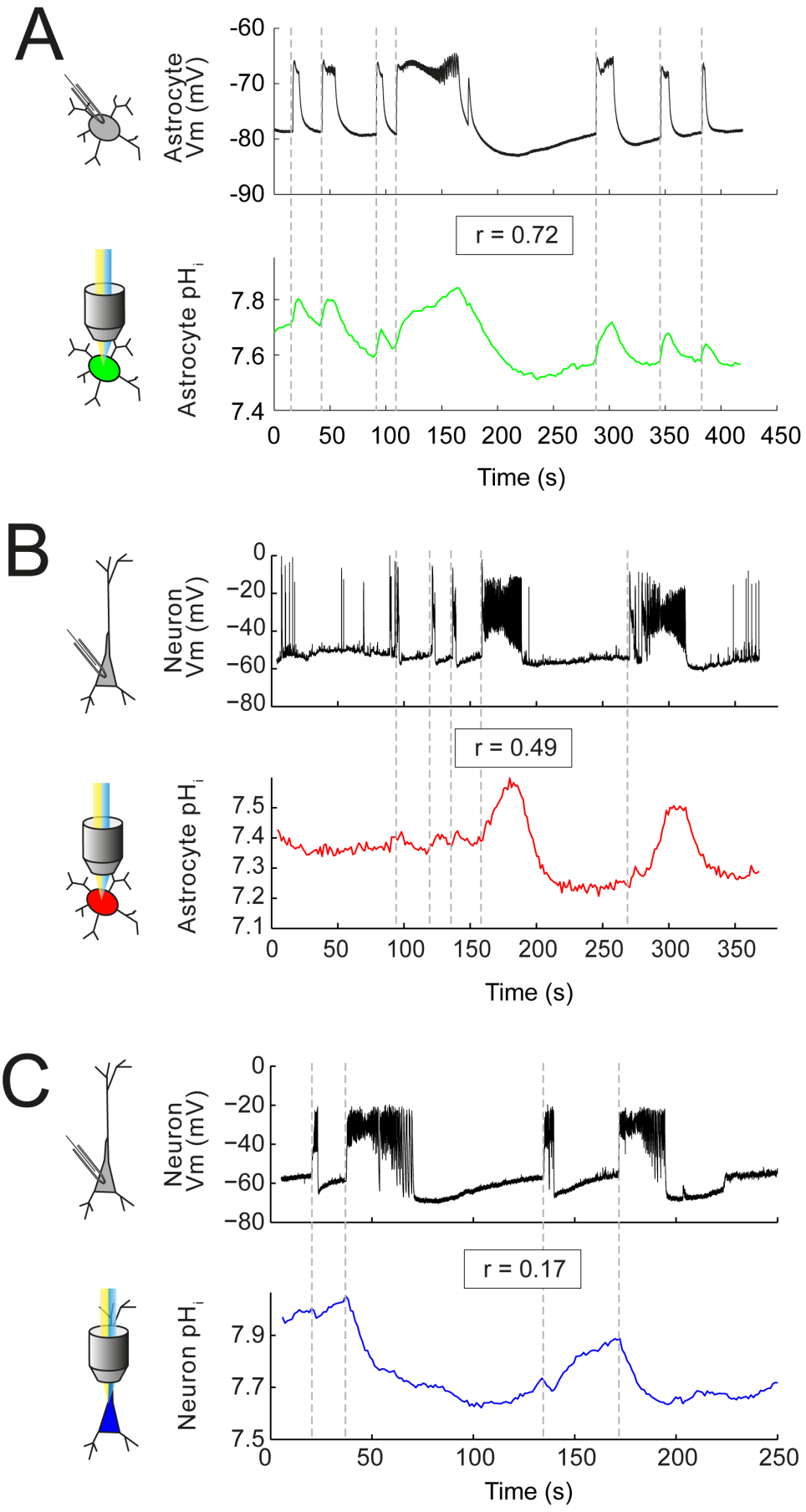

Figure 6: Simultaneous recordings from different cell-pair combinations reveal that astrocytic pH dynamics closely reflect both astrocytic and neuronal membrane potential dynamics

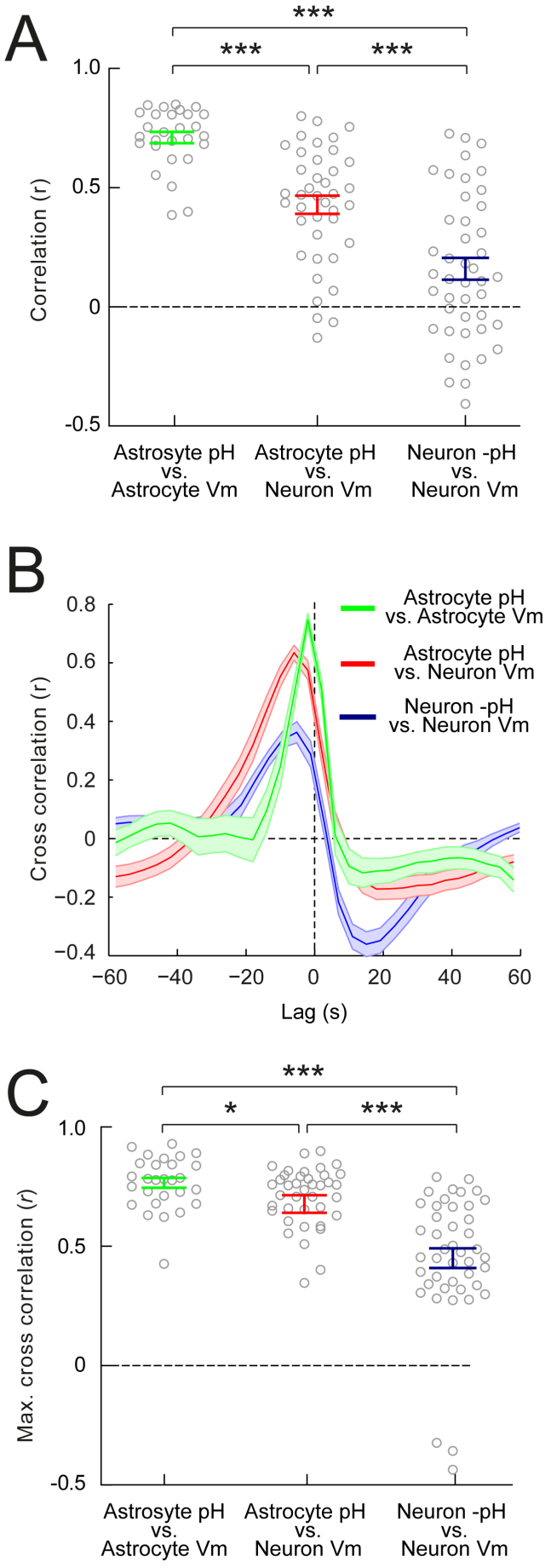

Figure 7: Astrocytic pH dynamics are more strongly coupled to network activity than neuronal pH dynamics